

Apparatus for Measuring Strength in Biaxial Compression^{a)}J. L. Belof¹ and J. I. Katz²¹⁾*Lawrence Livermore National Laboratory, Livermore, Cal. 94550*²⁾*Los Alamos National Laboratory, Los Alamos, N. Mex. 87545^{b)}*

(Dated: 8 June 2021)

Most measurements of compressive strength of ductile materials have involved Hopkinson-Kolsky bars or Taylor anvils placing samples in uniaxial compression. In these geometries strain is limited by the tendency of the sample to petal, in analogy to necking in uniaxial tension. Estimation of strength for any other form of the stress tensor requires assuming a shape for the yield surface; because data exist only for uniaxial compression these assumptions are untested. In an imploding spherical shell compression is biaxial, the plastic strain may not be small and the material behavior may be nonlinear as a result of work hardening and heating by plastic work. We propose to measure the strengths of materials in biaxial compression, both quasistatically and dynamically, using the compression of thin spherical shells. We suggest surrounding the shell with an annulus filled with a mixture of H₂ and Cl₂ gases whose volumetric detonation is initiated by a flash of blue and near-ultraviolet light. Less promising approaches are described in appendices.

PACS numbers: 62.20.-x, 81.70.Bt

Keywords: Strength of materials, biaxial compression

^{a)}Email: katz@wuphys.wustl.edu^{b)}Also at Department of Physics and McDonnell Center for the Space Sciences

Washington University, St. Louis, Mo. 63130

I. INTRODUCTION

The strengths of materials in compression, particularly at higher strain rates, are conventionally measured by the Hopkinson-Kolsky method¹⁻³. A thin sample is placed between the flat ends of two bars (an incident and a transmission bar) of strong material, and a pressure pulse is transmitted through the incident bar to the test sample. If the pulse is strong enough, the sample, subjected to a uniaxial compressive stress, flows plastically. Its compressive yield strength is the minimum compressive stress that produces plastic deformation. Simple analysis requires that the deformation be small, but small deformation is sufficient to determine the stress threshold for plastic flow (the yield stress). Alternatively, a flat-ended cylindrical bar of the test material impacts a thick slab of much stronger material, called a Taylor anvil⁴, and the threshold speed of impact at which the test material deforms plastically determines its compressive strength.

To apply these results to stress states other than uniaxial compression requires assuming a shape for the yield surface. Many shapes have been proposed; the most popular is probably that of von Mises:

$$(\sigma_1 - \sigma_2)^2 + (\sigma_2 - \sigma_3)^2 + (\sigma_3 - \sigma_1)^2 = 2S_u^2, \quad (1)$$

where the σ_i are the principal components of the stress tensor and S_u is the uniaxial yield strength (of a ductile material). The validity of this expression implies (or assumes) that the tensile and compressive yield strengths are equal. This is generally true for ductile materials, but is wrong for brittle materials which have low tensile yield strengths as a result of stress concentration at Griffith cracks; the von Mises criterion assumes ductility and a homogeneous (on scales smaller than sample feature sizes) stress field. In pure shear the yield strength is $\frac{1}{2}S_u$; this is obtained from the definition of shear stress $\tau = (\sigma_1 - \sigma_3)/2$ where σ_1 and σ_3 are respectively the major and minor principal stresses.

The validity of the von Mises yield surface is a fundamental question in materials science. Its simplest and most important test is to compare the yield stresses in unconfined uniaxial and in biaxial compression. The corresponding geometries are the Hopkinson-Kolsky bar in uniaxial compression and a thin spherical shell subjected to a uniform inward force or impulse that create biaxial compression. Once the yield strength is exceeded the material flows plastically, and the relation between the applied forces and its final deformation is determined by its strength. Measurement of its deformation and knowledge of the applied loads

permit determination of its strength. We propose to apply this method to the compression of thin spherical shells of ductile materials such as lead, tin and copper.

A number of means of supplying momentum and energy to stress a spherical shell and compress it may be considered. These include explosives, sparks, flyer plates, resistive heating of a driving fluid, gas pressure and piezoelectrics. Most of these methods suffer from difficulty in maintaining the necessary symmetry; a thin test shell subject to asymmetric loading will dimple, and even a symmetrically loaded shell may be subject to buckling instability.

We have considered a number of methods of loading a spherical test object:

1. Piezoelectric drive is not strong enough to produce plastic flow in all but the very weakest materials or in impractically thin shells.
2. Light initiated high explosives (LIHE), sprayed on as thin coats, can be well matched to the strengths of transition metals, determining their yield thresholds under dynamic biaxial compressive loads at interesting values of strain rate. However, it difficult to make these coats uniform to better than 20%, so that LIHE-driven thin shells are likely to crumple rather than to retain their spherical geometry.
3. A liquid metal “hydraulic fluid” surrounding the test shell might be pressurized by a spark or a tiny explosive or spark. However, the resulting weak shock would reverberate with very little damping as it propagates from its point sources, and the test object would be loaded asymmetrically, and be likely to crumple rather than to retain its spherical geometry.
4. We suggest that the most promising method is to surround the test shell with an explosive mixture of H_2 and Cl_2 , detonated homogeneously by a flash of blue or near-ultraviolet light.

Before describing these methods, we provide a general analysis of strength measurements. Then we describe the H_2 - Cl_2 explosive method in detail. The less promising methods 1–3 are described in appendices.

II. MEASUREMENT OF UNIAXIAL STRENGTHS

Extant measurements of uniaxial compressive strengths are generally based on data obtained from split Hopkinson bar, Taylor anvil (a hard surface that stops a high velocity cylinder of the material tested), or shock measurements. In the first two methods an unconfined test object is subjected to uniaxial compression and flows plastically in the unconfined directions. The achievable strain is limited by the finite tensile strain at rupture of even ductile materials. In uniaxial compression at high strains the plastically deforming material undergoes a petaling instability in which azimuthal asymmetry grows until the outer parts of the test object break into separate petals. The strain diverges at the apex of an opening crack between the petals but remains small within them.

In order to achieve a yield stress σ the longitudinal velocity in a Hopkinson bar or Taylor anvil experiment must be

$$v_l = \frac{\sigma}{Z_l}, \quad (2)$$

where $Z_l = \rho c_l$ is the longitudinal acoustic impedance and c_l the unconfined longitudinal wave speed. At higher v_l the material flows plastically; σ may increase as a result of work hardening, or decrease as a result of heating by plastic work. The characteristic time for a strain ϵ and displacement ϵr of a cylinder of radius r is

$$t_{char} = \frac{\epsilon r}{v_l} \sim \frac{\epsilon r Z_l}{\sigma}. \quad (3)$$

The corresponding strain rate is

$$\dot{\epsilon} \sim \frac{\epsilon}{t_{char}} \sim \frac{\sigma}{r Z_l}. \quad (4)$$

Representative numbers for a transition metal are $\sigma = 3$ kbar, $r = 0.1$ cm, $\rho = 8$ gm/cm³ and $c_l \approx c_s \approx 3$ km/sec, yielding a characteristic

$$\dot{\epsilon} \sim 10^4 \text{ s}^{-1}. \quad (5)$$

This is a practical upper limit on achievable values of $\dot{\epsilon}$. For very soft metals like indium the corresponding limits on $\dot{\epsilon}$ may be smaller by as much as two orders of magnitude.

The strength of ductile metals is generally an increasing function of their strain rate⁵⁻⁹, particularly at strain rates $> 10^3 \text{ s}^{-1}$. High strain rates $\dot{\epsilon}$ imply high dislocation velocities⁹

$$v_{disc} = \frac{\dot{\epsilon}}{n_{disc} a}, \quad (6)$$

where n_{disc} is the dislocation density and a is an interatomic spacing. The dislocation density may be as small as $\sim 10^7/\text{cm}^2$ in annealed metals or as large as $\gtrsim 10^{11}/\text{cm}^2$ in cold-worked metals¹⁰. A low-melting soft metal like indium ($T_m = 430$ K) is likely to anneal at room temperature and to have n_{disc} in the lower end of this range. Even Sn ($T_m = 505$ K) and Pb ($T_m = 600$ K) recrystallize at room temperature, although not on the ms time scale of a dynamic experiment. As v_{disc} increases, phonon drag on the dislocation increases rapidly and replaces pinning as the principal impediment to dislocation motion. This emphasizes the importance of obtaining strength data at strain rates of interest because the dependence of strength on strain rate is significant.

In shock experiments^{11–13} the pullback from shock reflection at a free surface measures the tensile strength of the material in its post-shocked (heated and damaged by plastic flow) state. The strain rates are subject to similar limitations as those in compressional experiments because the material velocities are similarly limited if it is required that the shock not far exceed the spall limit. The test rod thickness is replaced by the slab thickness. Shock experiments are, in general, harder to interpret quantitatively than unshocked experiments on bars.

III. EFFECT OF GEOMETRY

The stress field in a split Hopkinson bar experiment is uniaxial compression (unconfined in the the two transverse dimensions), in a shock experiment it may be uniaxial and slab-symmetric (transversely confined on the experimental time scale) tension, and in a converging thin spherical shell it is biaxial compression (unconfined in the radial direction). As a result, these are not directly comparable, and none may be directly applicable in other circumstances.

The stress tensor at yield in uniaxial compression, assuming the von Mises yield criterion (Eq. 1) is

$$\boldsymbol{\sigma} = S_u \text{sgn}(P) \left\{ \begin{vmatrix} 1 & 0 & 0 \\ 0 & 0 & 0 \\ 0 & 0 & 0 \end{vmatrix} = \frac{1}{3} \mathbf{1} + \begin{vmatrix} \frac{2}{3} & 0 & 0 \\ 0 & -\frac{1}{3} & 0 \\ 0 & 0 & -\frac{1}{3} \end{vmatrix} \right\}, \quad (7)$$

where P is the applied uniaxial pressure¹⁴¹.

¹ *N. B.:* S_u may be an increasing function of the isotropic pressure, the first Cauchy invariant I_1 . Such a

The stress tensor at yield of a thin spherical shell of thickness δr and radius r_0 loaded by an external pressure P , to lowest order in $\delta r/r_0$ and assuming the von Mises yield criterion, is

$$\boldsymbol{\sigma} \approx S_u \operatorname{sgn}(P) \left\{ \begin{vmatrix} 0 & 0 & 0 \\ 0 & 1 & 0 \\ 0 & 0 & 1 \end{vmatrix} = \frac{2}{3} \mathbf{1} + \begin{vmatrix} -\frac{2}{3} & 0 & 0 \\ 0 & \frac{1}{3} & 0 \\ 0 & 0 & \frac{1}{3} \end{vmatrix} \right\}. \quad (8)$$

The components $\sigma_{\theta\theta} = \sigma_{\phi\phi} \approx Pr_0/(2\delta r)$, while $\sigma_{rr} = \mathcal{O}(P)^{15}$. According to the von Mises criterion, yield begins at

$$P \approx \frac{2\delta r}{r_0} S_b \ll S_b, \quad (9)$$

defining the biaxial yield stress S_b . Eq. 1 implies that $S_b = S_u$ and that these yield strengths are the same in tension as in compression. The compressive stress is biaxial to lowest order in $\delta r/r_0$.

The deviatoric parts of the stress tensor differ in these two geometries. For compressive loads ($P > 0$) two components are negative in uniaxial compression, while only one is negative in biaxial compression. The compressive isotropic part of the stress tensor is twice as large in spherical compression, and acts to prevent petaling or spall. In the plastic flow of a bar in longitudinal compression the circumferential and radial length elements grow, while in the spherical compressive flow of a shell all non-radial length elements shrink and only the one radial dimension of length element grows.

A ductile compressively loaded bar petals at large strains, similarly to the necking of a bar in longitudinal tension. Stress and flow are greatest where the material is thinnest, leading to further thinning, increasing strain where it is thinnest, and finally to rupture if the limiting plastic strain is reached. In comparison, in the spherical shell only radial length elements stretch, and the opening of cracks and voids is prevented both by the (small) radial compressive load and the greater isotropic compressive stress.

The von Mises yield surface (Eq. 1) is an assumption that requires empirical justification. Is the value of yield stress S_u found for uniaxial compression also applicable to biaxial compression, as implied by Eq. 1? Two dimensional compression of a thin spherical shell is expected to be immune to petaling instability, and in the plastic flow regime immune

dependence in granular materials, in which friction resists plastic flow and that get much stronger under compression, is described by a Mohr-Coulomb yield surface. In ductile materials, for $I_1 \ll K$ (K is the bulk modulus) the density is close to that of the uncompressed state and the dependence of S_u on I_1 is expected to be weak.

to elastic buckling instability. By comparison to the strength measured in one dimensional compression it can provide a direct test of the validity of the von Mises yield surface. It can also measure such phenomena as the strain rate dependence of the strength and work hardening.

IV. SPHERICAL SHELLS

We consider the dynamics of a spherical shell impulsively launched inward whose initial kinetic energy is dissipated as heat by plastic work. In general, this is a nonlinear problem that requires numerical calculation. Here we present analytic results for the simplest possible case, a shell that remains thin, without its strength changing as a result of work hardening or plastic heating.

A. Motion

First consider a thin spherical shell of incompressible matter of mass M , density ρ , mean radius r and thickness $\delta r \ll r$, undergoing radial flow with slowly varying kinetic energy E . Its mean mass-averaged radial velocity v_m also varies slowly. However, its thickness changes with time. To lowest order in $\delta r/r$:

$$\delta r \approx \frac{M}{4\pi\rho r^2}, \quad (10)$$

and

$$v_m \approx \sqrt{\frac{2E}{M}}. \quad (11)$$

The speeds of its surfaces are

$$v_{\pm} \approx v_m \left(1 \mp \frac{\delta r}{r} \right), \quad (12)$$

where the upper signs refer to the outer surface and the lower signs to the inner surface.

The accelerations of its surfaces are

$$a_{\mp} \approx \pm 3 \operatorname{sgn}(v_m) \frac{\delta r}{r} \frac{v_m^2}{r}. \quad (13)$$

In an imploding flow the speed of the inner surface increases and that of the outer surface decreases. In an expanding flow the opposite is true.

B. Plastic work

For a thin spherical shell that has undergone a change in radius δr in radial incompressible flow, the diagonalized strain tensor in local cartesian coordinates of an element

$$\mathbf{u} = \begin{vmatrix} \frac{d\delta r}{\delta r} & 0 & 0 \\ 0 & -\frac{d\delta r}{2\delta r} & 0 \\ 0 & 0 & -\frac{d\delta r}{2\delta r} \end{vmatrix}. \quad (14)$$

Using the expressions for stress (8) and strain (14), the plastic work (ignoring the elastic deformation) per unit volume of the shell

$$dW = \mathbf{u} \cdot \boldsymbol{\sigma} = -S_b \frac{d\delta r}{\delta r}. \quad (15)$$

Integrating, noting that $\delta r \propto R^{-2}$ where R is the shell's radius,

$$W = \int dW = 2S_b |\ln(R_i/R_f)|, \quad (16)$$

where R_i and R_f are the initial and final radii.

V. BIAXIAL STRENGTH

Yield strength in biaxial compression is of intrinsic interest because it offers the opportunity to test models of the yield surface. This geometry can also enable measurement of strength at high strain (because of the absence of the petaling instability that occurs in uniaxial compression) and at high strain rate.

A. Quasistatic Compression

The strength of a thin shell in biaxial compression at low strain rates can be measured using hydraulic compression. A thin spherical shell of the material to be tested is placed in a chamber filled with hydraulic fluid. This chamber is thick-walled with a stiff material such as steel, so that its deformation is negligible. If the test object has a small volume compared to that of the chamber then the volume of the chamber remains essentially constant even as the test object shrinks to smaller volume (the shrinkage is of its central void; the metal is essentially incompressible). A schematic diagram of the experiment is shown in Fig. 1.

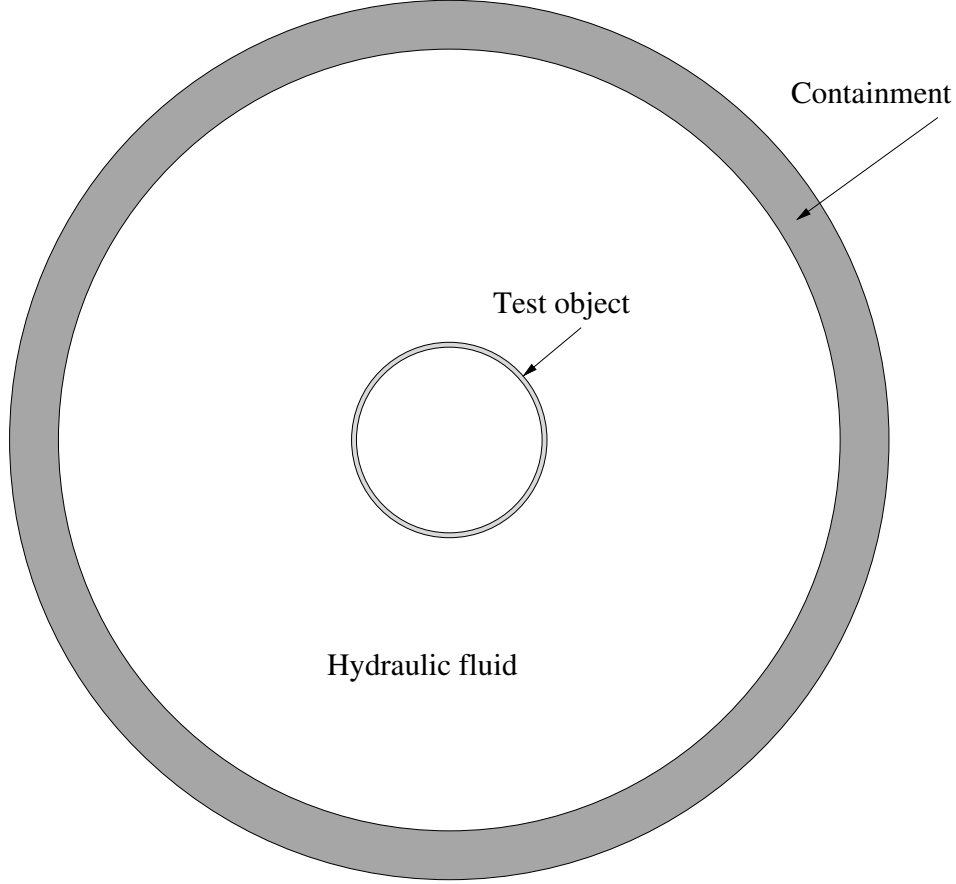


FIG. 1: Schematic of quasi-static biaxial compression experiment.

The stress in the test object

$$\sigma = \frac{pR}{2\delta r}, \quad (17)$$

where p is the external pressure, R is its radius and $\delta r \ll R$ is the thickness of its shell. As it compresses at constant p and constant density, the shell thickens $\delta r \propto R^{-2}$, so the pressure threshold for plastic flow

$$P_{thresh} = \frac{2S_b\delta r}{R} \propto R^{-3}, \quad (18)$$

where S_b is the biaxial compressive yield stress of the shell. The increase of P_{thresh} with decreasing R makes compression stable, provided the shell remains spherical. Compression is quasi-static as the pressure of the hydraulic fluid is increased². Work-hardening may make P_{thresh} increase even faster than $\propto R^{-3}$.

² Expanding the shell with an internal gas is only neutrally stable on the (slow) time scales on which the gas is isothermal because $P_{thresh} \propto V^{-1}$ while the internal pressure of an isothermal gas is also $p \propto V^{-1}$. On faster (dynamic) time scales $p \propto V^{-\gamma}$, where $\gamma > 1$ is the adiabatic index, and is stable provided spherical

In order to maintain, to a good approximation, a constant pressure during this process, the hydraulic pump (not shown in the Figure) must respond to the shrinkage of the test object on the time scale on which it shrinks. Because an infinitesimal overpressure produces an infinitesimal shrinkage, provided the plastic flow of the test object is ductile, this condition is expected to be met.

It may be attractive to use very thin shells to minimize the pressure required to produce plastic work (Eq. 18). However, if the shell is too thin the possibility of buckling must be considered. Buckling of a elastic thin perfectly spherical shell occurs at a pressure¹⁵

$$P_{buckle} = \frac{2E}{\sqrt{3(1-\nu^2)}} \left(\frac{\delta r}{R} \right)^2, \quad (19)$$

where E is the Young's modulus and $\nu \approx 0.3$ the Poisson's ratio of the shell. Combining this with Eq. 18 yields the condition that the shell not buckle at its plastic yield threshold

$$\frac{\delta r}{R} > \frac{S_b}{E} \sqrt{3(1-\nu^2)} \sim 0.001-0.005, \quad (20)$$

where typical parameters for transition metals have been used. However, such very thin shells may buckle as a result of deviations from perfect sphericity and may be difficult to handle without damage. For these practical reasons it will probably be necessary to use shells at least ten times thicker than those permitted by Eq. 20; this equation then demonstrates that spherical elastic buckling will not occur.

B. Dynamic Compression

Consider an impulse per unit area p_f applied to a thin spherical shell of the sample material of density ρ , initial radius R_i and thickness δr . Equating the kinetic energy per unit volume $p_f^2/2\rho(\delta r_0)^2$, where δr_0 is the initial shell thickness, to the plastic work (16) done before the shell stops at a final radius R_f , yields a relation between its yield strength S_b and R_i/R_f , with the other variables as parameters:

$$S_b = \frac{p_f^2}{4\rho(\delta r_0)^2 |\ln(R_i/R_f)|}. \quad (21)$$

symmetry is maintained. In fact, expansion by an internal fluid is unstable to dynamical non-spherical instability: any weaker or thinner part of the shell will stretch preferentially, with the expansion occurring disproportionately there. Catastrophic rupture will be almost immediate. It is only possible to inflate a rubber balloon without rupture because of the nonlinear stress-strain relation of rubber: After a 2-3 fold stretch it becomes much stiffer.

It is probably best to choose an impulse so that $\ln(R_i/R_f) \lesssim 0.5$, preserving the spherical geometry of the shell even if the implosion is not very accurately spherical. For $S_b = 1$ kbar (a plausible value for a transition metal), $\delta r_0 = 1$ mm, $R_f = 0.6R_i$ and $\rho = 8.9$ g/cm³ (copper) and defining $\delta \equiv (R_i - R_f)/R_i$, if $\delta \ll 1$ the required impulse per unit area

$$p_f \approx 1.9 \times 10^4 \sqrt{\delta} \text{ taps}, \quad (22)$$

where $1 \text{ tap} \equiv 1 \text{ g cm}^{-1} \text{ s}^{-1}$ is the cgs unit of impulse per unit area.

The radial strain rate varies during the trajectory of the shell, but may be approximated

$$\dot{\epsilon}_r \approx \frac{\epsilon_r}{t_{char}} \approx \frac{2p_f}{R_i \rho \delta r_0} \approx 4 \sqrt{\frac{S_b \delta}{\rho}} \frac{1}{R_i} \approx 2 \times 10^4 \text{ s}^{-1}, \quad (23)$$

where the radial strain $\epsilon_r \approx 2(R_i - R_f)/R_i$, the characteristic time $t_{char} \approx (R_i - R_f)/v$ and the initial velocity $v = p_f/(\rho \delta r_0)$. The final result uses Eq. 22 for the impulse per unit area p_f and the numerical values $S_b = 1$ kbar, $\rho = 8.9$ g/cm³, $\delta = 0.3$ and $R_i = 1$ cm. The strains and strain rates in the two tangential dimensions are half as large.

VI. EXPERIMENTAL METHOD: HYDROGEN-CHLORINE EXPLOSIONS

The explosive reaction of hydrogen and chlorine



may be initiated by blue or near-ultraviolet light, and is explosive. This suggests a means of applying a nearly impulsive pressure to a test shell, as shown in Fig. 2. The reason for choosing a hydrogen-chlorine reaction rather than the more familiar explosive hydrogen-oxygen reaction



is the ease of photoinitiating the hydrogen-chlorine explosion, permitting the simultaneous and uniform development of overpressure. The hydrogen-oxygen explosion is generally initiated by a spark, and a detonation front propagates in a complex and asymmetric manner from the point of initiation.

Blue or ultraviolet light dissociates Cl_2 molecules, leading to the chain reaction



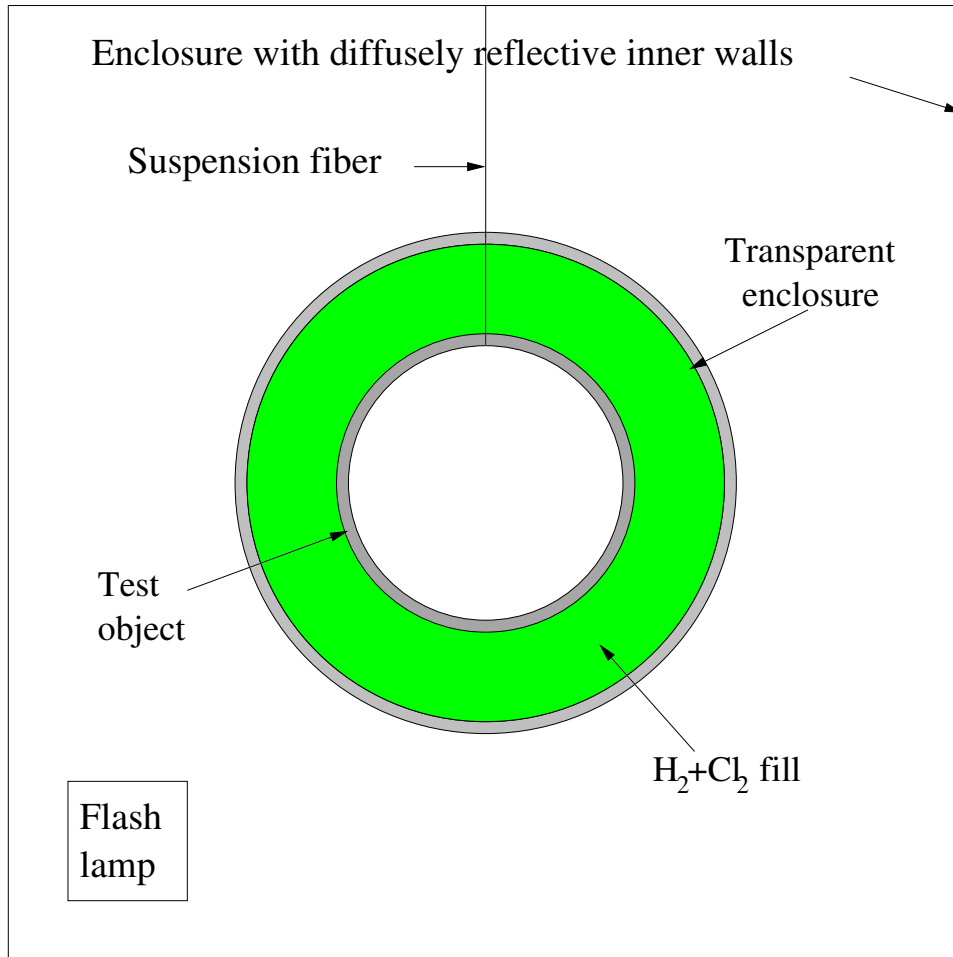


FIG. 2: Photo-induced detonation of a mixture of H_2 and Cl_2 applies a very rapidly rising pressure to the test object. Flooding the enclosure with blue or near-ultraviolet light initiates all the explosive mixture simultaneously, ensuring symmetry of the applied pressure, provided the transparent containment vessel is spherical and concentric with the test object. If the containment vessel is frangible, the suddenly released pressure will fragment it into many small fragments, and the high pressure HCl gas will rapidly escape between the fragments, reducing the pressure by a large factor. The load on the test object will be nearly impulsive on the time scale of its motion.

Reaction 26 is endothermic by an energy (in temperature units) of about 600 K, small enough that it is readily supplied by thermal energy at room temperature, while reaction 27 is exothermic by about 22740 K, yielding a net enthalpy of reaction of about 11070 K per HCl molecule. These exchange reactions have large cross-sections $\sigma \sim 10^{-16} \text{ cm}^2$.

This is not a branching chain, and may be terminated by reactions



The bystander R is necessary because the rate of radiative association is very small in these reactions that have no dipole moment. As a result, it is necessary that a non-infinitesimal fraction of the Cl_2 be photodissociated. Once a significant amount of product HCl has been produced, the temperature rises sufficiently that the chain branches by the reaction



which is endothermic by 29120 K (2.51 eV), and rapidly proceeds to completion.

The characteristic reaction time at an initial pressure P

$$t_{\text{char}} = \frac{1}{n\sigma_{\text{react}}v_{\text{th}}} \sim 3 \frac{1 \text{ bar}}{P} \text{ ns}, \quad (31)$$

where we have taken a reaction cross-section $\sigma \sim 10^{-16} \text{ cm}^2$, n is the reactant density and $v_{\text{th}} \sim 10^5 \text{ cm/s}$ is the thermal velocity of the hydrogenic species at room temperature. Once the chain is initiated, it rapidly proceeds to completion. These reactions have been studied in detail because of their significance for the chlorine industry in which electrolytically produced chlorine is mixed with some hydrogen; see¹⁶ for a bibliography.

A. Radiative Initiation

In order to assure uniform volumetric initiation it is necessary that the entire volume be illuminated. The level diagram of the Cl_2 molecule and its photoabsorption cross-section are shown in Fig. 3.

Near the near-ultraviolet absorption peak, the attenuation at $P_{\text{Cl}_2} = 5 \text{ bars}$ (as discussed in Sec VIB pressures in this range are relevant) is $\sim 25 \text{ cm}^{-1}$, so the illumination would not penetrate very deep into the gas. However, the attenuation at longer (blue and green) wavelengths is much less, so this light from a broad-spectrum source would penetrate through the gas and initiate the reaction in the inner regions of the gas-filled annulus. The product HCl is transparent at visible and near-ultraviolet wavelengths with $\lambda > 2270 \text{ \AA}$ ¹⁹.

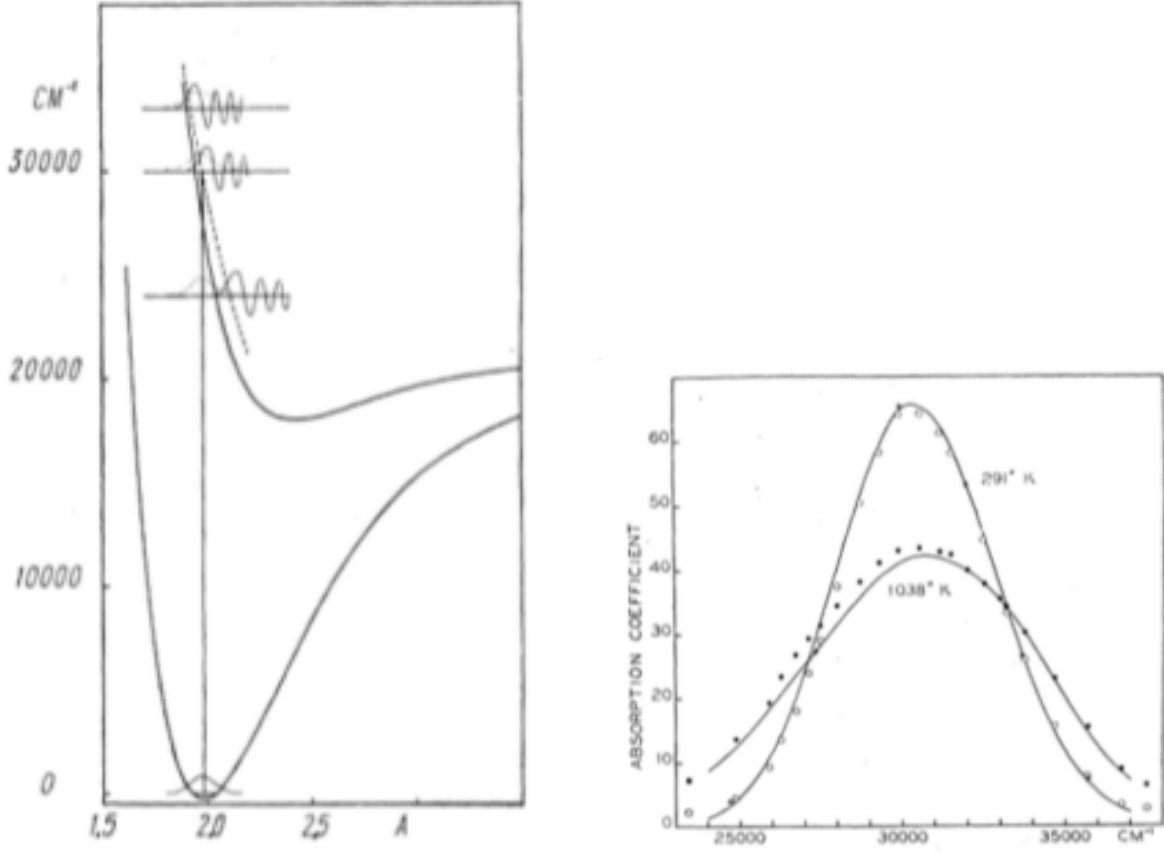


FIG. 3: Left subfigure shows the level diagram of the Cl_2 molecule. The solid lines show the Morse potentials of the ground $X \ ^1\Sigma_g^+$ state and the first excited $^1\Pi_u$ state with an allowed transition. Because of the Franck-Condon principle, excitation from the ground state has large matrix element only into unbound high vibrational levels of the excited electronic state at shorter wavelengths than the $\lambda = 4915 \text{ \AA}$ corresponding to the dissociation threshold of 2.51 eV. The right subfigure shows the absorption coefficient as a function of reciprocal wavelength, in units of $(\text{dex/cm})/(\text{moles/l})$ at 291 K; multiply by 0.1004 to transform to $\text{cm}^{-1}(P_{\text{Cl}_2}/\text{bar})$ for Cl_2 partial pressure P_{Cl_2} at 298 K^{17,18}.

B. Pressure Multiplication

In order to force a shell of thickness δr and initial radius R_i to flow plastically, in a static approximation a pressure $P = 2Y\delta r/R_i$ is required, where Y is the yield stress. For plausible parameters for a soft transition metal $Y = 1 \text{ kbar}$ and $\delta r/R_i = 0.05$; $P = 100 \text{ bars}$ would be required. The criterion is more complicated for dynamic loading (Sec. V B).

There is a simple relation between the gas pressure before ignition of a stoichiometric

mixture and afterward:

$$\frac{P_f}{P_i} = \frac{\Delta H}{k_B T_i} \frac{2}{n}, \quad (32)$$

where ΔH is the enthalpy of reaction, T_i the initial gas temperature, n the number of effective degrees of freedom of the burned gas and the molar ratio is 1 for the reaction $H_2 + Cl_2 \rightarrow 2HCl$ but $2/3$ for the reaction $2H_2 + O_2 \rightarrow 2H_2O$. The enthalpy for the chlorine reaction is 92.34 kJ/mole (HCl), while for the oxygen reaction it is 242 kJ/mole (H_2O); these values assume complete reaction, which is in fact an overestimate by about 15% for the chlorine reaction and by more for the oxygen reaction. For HCl $n \approx 6.5$ (Sec. VIB 1), while for H_2O , a nonlinear triatomic molecule produced with large ΔH , all nine degrees of freedom may be approximated as classically excited. The resulting pressure ratios (with $T_i = 298$ K) are

$$HCl \quad \frac{P_f}{P_i} = 11.5 \sim 10 \quad (33)$$

$$H_2O \quad \frac{P_f}{P_i} = 21.7 \sim 10, \quad (34)$$

where the final approximate values allow for the fact, discussed in Sec. VIB 2, that the reactions don't go to completion because of the high temperatures of the product gases. These reactions, explosively turning gases into other gases, may be thought of as pressure multipliers. The greater ΔH of the oxygen reaction is partially offset by the greater number of degrees of freedom of its products.

1. Degrees of Freedom

At the temperatures produced by reaction (24), a few thousand K, the quantized nature of the vibration of HCl, with a level spacing of 2991 cm^{-1} ¹⁹ (implicitly multiplied by hc so that 1 cm^{-1} corresponds to 1.986×10^{-16} erg), or 4304 K in temperature units), is important. The total vibrational energy per molecule is

$$\mathcal{E} = h\nu e^{-h\nu/k_B T} + 2h\nu e^{-2h\nu/k_B T} + \dots = \frac{e^{-h\nu/k_B T}}{(1 - e^{-h\nu/k_B T})^2}. \quad (35)$$

The energy balance equation

$$\Delta H = 5k_B T + 2\mathcal{E}, \quad (36)$$

where the first term is the contribution from the three translational and two rotational degrees of freedom and ΔH describes reaction (24) with two moles of HCl on the right hand

side, may be solved numerically (by successive approximation) for T . Then the effective number of vibrational degrees of freedom is

$$n_{vib} = 2 \frac{\mathcal{E}}{k_B T} \quad (37)$$

and

$$n = 5 + n_{vib}. \quad (38)$$

2. *Completeness of Reaction*

For the reaction (24) the final temperature, ignoring the (small) contribution of the initial thermal energy, is simply related to ΔH :

$$k_B T = \frac{\Delta H}{n}. \quad (39)$$

As a result, for a stoichiometric gas mixture the final HCl density n'_{HCl} can be related to the residual H_2 density $n'_{H_2} = n'_{Cl_2}$:

$$\frac{n'^2_{HCl}}{n'_{H_2} n'_{Cl_2}} = e^{\Delta H / k_B T}. \quad (40)$$

This may be solved for the reaction (24) to yield

$$n'_{HCl} = \frac{n_{H_2}}{1/2 + e^{-\Delta H / 2k_B T}}, \quad (41)$$

where an unprimed variable indicates the pre-reaction density. After solving for T we find

$$n'_{HCl} = 1.83 n_{H_2}; \quad (42)$$

about 8.6% of the initial reactants remain unreacted. This reduces the energy released by a similar amount.

An analogous, but more complicated (because the number of molecules is changed by the reaction) calculation can be performed for reaction (25). The fractional reduction in energy yield is greater than for reaction (24) because the greater number of momentum states accessible to the greater number of reactant molecules shifts the equilibrium to the left. This is analogous to the fact that a gas is 50% ionized at temperatures far below those corresponding to the ionization energy. Some results are reported in²⁰, who found that for a stoichiometric mixture H_2O constituted barely 50% of the mole fraction of the product gas.

C. Frangible Gas Containment

We typically want to apply an impulsive load to a test spherical shell, as analyzed in Secs. IV and V B. This requires that the outer shell containing the $\text{H}_2\text{--Cl}_2$ mixture rapidly release the hot, high pressure, reaction products. Their sound speed is about 1 km/s so that an annulus 3 cm thick will decompress in tens of μs if the containment shell is frangible and breaks into many small fragments. This is much less than the time over which the test object flows plastically.

Candidate materials are glass and the brittle plastics polystyrene and PMMA, each of which have Weibull moduli $\sim 6\text{--}10$. Because they are brittle it is probably necessary that their static, pre-explosion, loads be several times less than their nominal tensile strengths Y , which are about 500–800 bars. For an internal pressure P_i and an acceptable stress σ the required fractional thickness of a spherical shell

$$\frac{\Delta R}{R} \geq \frac{1}{2} \frac{P_i}{\sigma}. \quad (43)$$

Taking $P_i = 20$ bars, sufficient to produce a post-explosion pressure $P_f \approx 200$ bars (Eq. 33) and a tolerable $\sigma = 200$ bars the required $\Delta R/R = 0.05$. These parameters may be scaled freely, but plausible values are $R = 5$ cm and $\Delta R = 2.5$ mm. The post-explosion pressure would produce, if confined, a static stress in the shell of 2 kbar, far in excess of its strength and ensuring immediate fragmentation.

In order to maintain symmetric pressure in the explosion products until they have vented and their pressure has become insignificant, the shell must fragment into pieces much smaller than the thickness of the annulus between it and the test object. This may be assured if the shell is scored by grooves, perhaps 5 mm apart, to guide its fragmentation. The grooves should be rounded to avoid stress concentration and fracture before the explosion. Brittle fracture occurs when the stress intensity at a crack or groove

$$K \approx \sigma \sqrt{\pi a}, \quad (44)$$

where a is a crack depth, exceeds the fracture toughness K_{IC} . For these plastics $K_{IC} \sim 10^8$ erg/cm^{5/2}. It is necessary that the material not fracture under the pressure of the reactant gas, so that

$$a < \frac{K_{IC}^2}{\pi \sigma^2} \lesssim 0.1 \text{ cm}. \quad (45)$$

Because the properties of brittle materials vary from sample to sample, this is only a rough guide, but establishes the feasibility of controlling the fracture in such a manner as to insure breakup into many small fragments, insuring approximately symmetric venting of the high pressure explosion products.

D. Numerical Example

If the initial total pressure of a stoichiometric mix of reactants is 30 bars, then the pressure after explosion will be about 300 bars, and the impulse delivered about 10 ktaps (1×10^4 g/cm-s). As discussed in Sec. IV B, this is an interesting regime for inducing two dimensional plastic flow in a thin sphere of ductile metal. A more quantitative result requires a code calculation, but this should be accurate to a factor of two.

VII. DISCUSSION

Many different yield surfaces have been proposed, of which von Mises's is probably the most popular for ductile materials. Unfortunately, because of the difficulty of measure compressive strength in any geometry other than uniaxial compression, there are few empirical grounds for preferring one yield surface to another. This paper proposes a method of measuring strength in two-dimensional compression that would provide an additional empirical parameter and constrain the yield surfaces of the tested materials.

The appendices discuss alternate means of applying impulsive loads to the outside of a thin spherical shell. These appear less promising, either because of the difficulty of ensuring symmetric loading or of providing sufficient impulse. They are included for completeness.

VIII. ACKNOWLEDGEMENT

This work was performed under the auspices of the U.S. Department of Energy by Lawrence Livermore National Laboratory under Contract DE-AC52-07NA27344 and by the Los Alamos National Laboratory, operated by Triad National Security, LLC for the National Nuclear Security Administration of the US Department of Energy under Contract 89233218CNA000001.

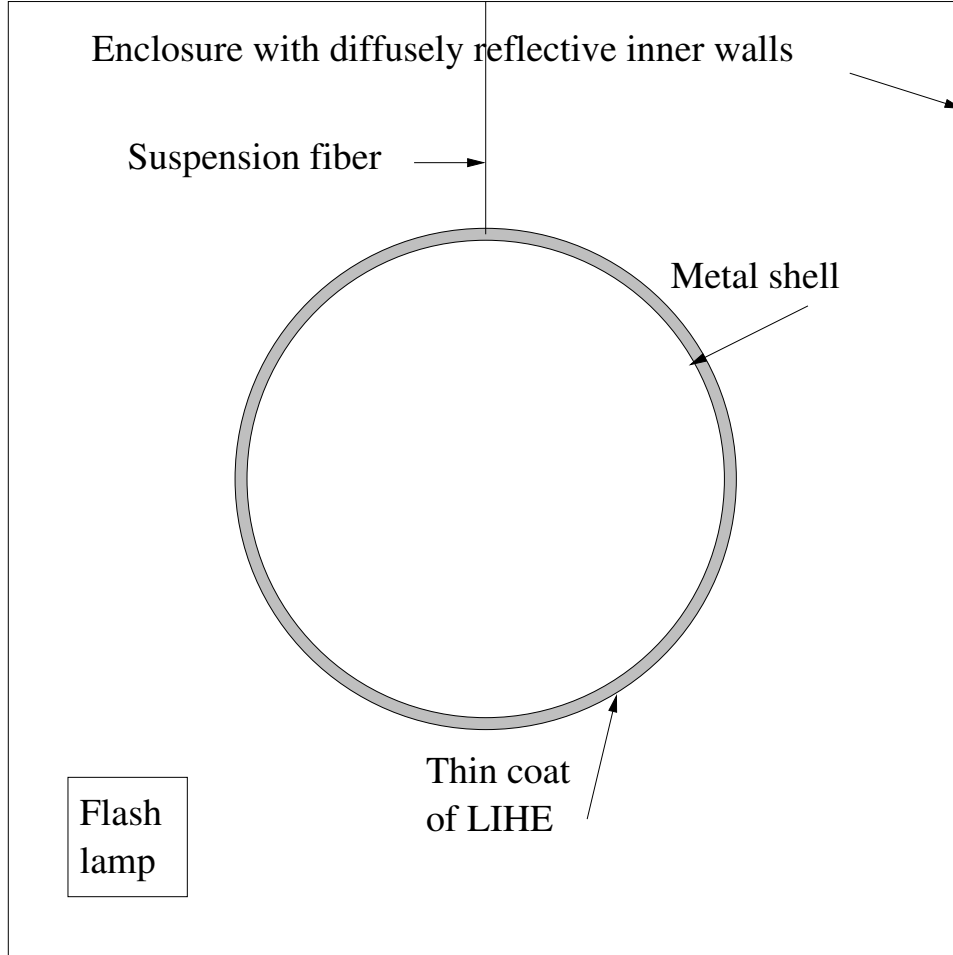


FIG. 4: Schematic of high strain rate LIHE biaxial compression experiment.

IX. DATA AVAILABILITY STATEMENT

This theoretical study produced no original data.

Appendix A: Light Initiated High Explosives (LIHE)

Light initiated high explosives^{21–24}, deposited in thin layers, are used to apply impulsive loads to the outside of a thin spherical shell. The thickness of the explosive layer is chosen so that it applies an impulse per unit area p_f to the shell. The required impulses (Eq. 22) are readily achievable. This is illustrated in Fig. 4.

The drawback of this method is that it is difficult to apply LIHE uniformly. It is typically estimated that nonuniformities are $\sim 20\%$. The effect of the resulting asymmetry of the

implosion would require two- (or three-) dimensional elastic-plastic flow calculations, beyond the scope of this paper, to evaluate. In particular, if the flow were to develop hinges the spherical description would become qualitatively invalid and results difficult to interpret. We have investigated the $\text{H}_2\text{-Cl}_2$ explosion method chiefly because it may more readily apply a symmetric load to the test object. However, if the asymmetry problem can be overcome, the LIHE method may be comparatively simple to implement.

Appendix B: “Hydraulic” Fluids

Pressure might be applied with a “hydraulic” fluid of high bulk modulus and sound speed, such as gallium or a gallium alloy of low melting point³. The fluid may be pressurized by the release of electrical or chemical energy or by the impact of flyer plates.

The fluid’s high sound speed would relax spatially asymmetric transients if they were strongly dissipative, but in the necessary regime of weak shocks dissipation is negligible and these weak shocks would reverberate in the “hydraulic” fluid rather than relaxing to a uniform pressure, providing asymmetric, rather than the spherically symmetric, compression required to prevent dimpling or crumpling. In addition, it is probably not possible to make sufficiently small explosive charges (small critical radii imply extreme sensitivity).

Appendix C: Piezoelectric Drive

Piezoelectric drive is relegated to this Appendix because saturation of dielectric response limits the impulse that can be delivered to levels insufficient to drive even a very soft metal like indium to plastic flow. However, the analysis is of intrinsic interest.

1. Symmetry

Piezoelectric drive is spherically symmetric if the driving electric field is produced between concentric spherical electrodes and if the piezoelectric ceramic is radially and spherically symmetrically poled. Spherically symmetric poling may be achieved by poling hemispherical shells that are later joined. Because the relative dielectric constant of PZT ceramics is

³ Galistan, the ternary gallium-indium-tin eutectic with its eutectic point below room temperature, may be the best candidate.

~ 1000 – 2000 the fringing fields at the hemispherical boundaries during poling are very small, and the poling is nearly symmetric. Alternatively, it might be possible to pole the entire spherical shell of piezoelectric with a floating inner electrode if the electrical conductivity of the piezoelectric is small enough. Very small conductivities are hard to measure, but extrapolation of conductivities measured at higher temperature²⁵ to typical poling temperatures of 100 – 160 C suggests that discharge times $t_{RC} = \epsilon/\sigma$, where here σ is the conductivity, may be as long as hours. Here we outline the design of such a piezoelectric-driven biaxial compression experiment.

Place a thin spherical shell of the test material, of density ρ , initial radius r_0 and thickness δr inside a spherical, radially poled, piezoelectric shell. Contain the piezoelectric within a stiff and strong containment shell. The containment shell serves several functions: it provides one of the electrodes required to apply an electric field to the piezoelectric, reflection of radial expansion of the piezoelectric by the shell provides an additional source of compression of the test object, and it contains the brittle piezoelectric if reflected pressure pulses create a tensile stress sufficient to fragment it. This is shown in Figure 5.

The electric discharge time of the floating inner electrode

$$t_{\text{discharge}} = \frac{\epsilon_0 \kappa}{\sigma}, \quad (\text{C1})$$

where $\kappa \approx 2000$ is the relative permittivity of the piezoelectric and $\sigma \approx 10^{-11}$ mho/m is its electrical conductivity²⁵. Then $t_{\text{discharge}} = \mathcal{O}(10^3)$ s, much longer than the duration of the dynamic phase of the experiment, so that no electric lead to the floating inner electrode is necessary. This preserves spherical symmetry. Aside from simplifying calculation and analysis, spherical symmetry reduces or eliminates any tendency of the test object to dimple, hinge, or otherwise deviate from uniform flow, as it might if subject to aspheric loading.

2. Equations

The equations of a piezoelectric ceramic, in engineering notation in which the subscript 3 denotes the radial (poled) direction, are

$$S_1 = s_{11}T_1 + s_{12}T_2 + s_{13}T_3 + d_{13}E_3 \quad (\text{C2})$$

$$S_2 = s_{21}T_1 + s_{22}T_2 + s_{23}T_3 + d_{23}E_3 \quad (\text{C3})$$

$$S_3 = s_{31}T_1 + s_{32}T_2 + s_{33}T_3 + d_{33}E_3, \quad (\text{C4})$$

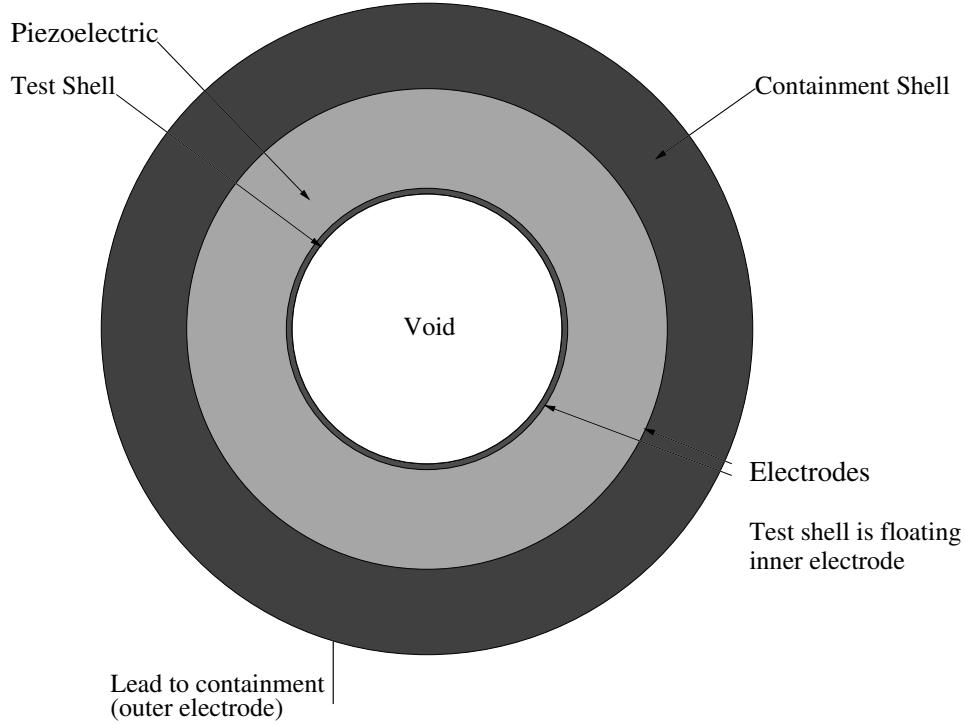


FIG. 5: Schematic of high strain rate piezoelectric compression apparatus. The containment shell and piezoelectric are made in two pieces that may be assembled before the shot, and disassembled afterward (the piezoelectric ceramic will likely shatter) to allow measurement of the plastic flow of the test object. The test shell and the containment shells are also the electrodes driving the piezoelectric. Piezoelectrics like PZT are sufficiently resistive that the test object/inner electrode can float electrically over the time of the experiment; it is not necessary to penetrate the piezoelectric with a lead wire to the test object/inner electrode.

where E_3 is the radial electric field, the S_i are the principal components of strain, the T_i are the principal components of stress, the s_{ij} are the components of the compliance tensor and the d_{ij} are piezoelectric coefficients. For a ceramic in which the 1 and 2 directions are equivalent $s_{11} = s_{22}$, $s_{12} = s_{21}$ and $s_{13} = s_{23}$. The s_{ij} are defined at constant electric field if the outer electrode is maintained at constant potential with respect to ground during the pulse that accelerates the test object (which is grounded by charge leakage prior to the experiment). The implied electric work done by or on the power supply is not considered explicitly.

For an instantaneously applied electric field $S_i = 0$ because the material has no time

to move. Solving for the stresses under these conditions, and simplifying by substituting components of the elasticity tensor c_{ij} for convenience, we find

$$T_1 = T_2 = E_3 d_{13} \left[\frac{1}{s_{11} + s_{12}} + c_{13} \left(\frac{d_{33}}{d_{13}} + 2 \frac{c_{13}}{c_{33}} \right) \right] \quad (C5)$$

and

$$T_3 = -E_3 (d_{33} c_{33} + 2 c_{13} d_{13}). \quad (C6)$$

The stress drop $T_3 - 0$ between the inside and outside of the test shell accelerates it inward.

The equation of motion of the test shell is

$$\frac{dp}{dt} = T_3 - \frac{c_{33}}{\delta r_{piezo}} \int \frac{p}{\rho \delta r} dt, \quad (C7)$$

where p is its momentum per unit area and we have made the approximation of only a small inward displacement, and therefore of constant thickness δr and radius r_0 . The second term arises from the reduction in stress in the piezoelectric as the test shell moves inward, sending a rarefaction into it, and makes the approximations that the piezoelectric thickness $\delta r_{piezo} \ll r$ and that it responds quasistatically to the motion of the test object. The final approximation is justified by the stiffness of ceramics: for PZT $c_{33} \approx 1.2 \times 10^{12}$ erg/cm³ and the sound speed is several km/s.

Differentiating again with respect to time

$$\frac{d^2 p}{dt^2} = -b^2 p, \quad (C8)$$

where

$$b \equiv \sqrt{\frac{c_{33}}{\rho \delta r_{piezo} \delta r}}. \quad (C9)$$

Using the boundary conditions $p = 0$ and $\frac{dp}{dt} = T_{30}$ at $t = 0$ we find the solution

$$p = \frac{T_{30}}{b} \sin bt. \quad (C10)$$

Equation C7 is only valid as long as the radial stress in the piezoelectric remains compressive:

$$\Delta P = T_{30} - \frac{c_{33}}{\delta r_{piezo}} \int \frac{p}{\rho \delta r} \geq 0. \quad (C11)$$

Once $T_3 < 0$ a void will open between the piezoelectric and the test shell, and the effective $T_3 = 0$, to good approximation. This happens after a time $t_{void} = \pi/(2b)$. After this time the test shell coasts inward, until all its kinetic energy is dissipated in plastic work.

The final momentum per unit area

$$p_f = \frac{T_{30}}{b}. \quad (\text{C12})$$

Equating the kinetic energy per unit volume $p_f^2/(2\rho(\delta r)^2)$ to the plastic work (16) done before the shell stops after an inward displacement $\Delta r \ll r_0$ yields a relation between S_b and Δr , with the other variables as parameters:

$$S_b = \frac{r_0}{\Delta r} \frac{T_{30}^2 \delta r_{piezo}}{4\delta r c_{33}}. \quad (\text{C13})$$

Equivalently, we may write the required initial piezoelectric stress

$$T_{30} = \sqrt{4S_b c_{33} \frac{\Delta r}{r_0} \frac{\delta r}{\delta r_{piezo}}}. \quad (\text{C14})$$

Inverting Eq. C13 yields estimates of useful ranges of the parameters. For a nominal transition metal (like copper or tin) of density $\rho = 9 \text{ gm/cm}^3$ with $\delta r = 0.1 \text{ cm}$ and $\delta r_{piezo} = 0.3 \text{ cm}$, the rate parameter $b = 2.1 \times 10^6/\text{s}$. The strain rate varies during the trajectory of the shell, but may be approximated

$$\dot{\epsilon} \approx \frac{\epsilon}{t_{void}} \approx \frac{4}{\pi} \frac{\Delta r}{r_0} b \approx 2.7 \times 10^5/\text{s}, \quad (\text{C15})$$

where the radial strain $\epsilon = 2\Delta r/r_0 = 0.2$; the strains and strain rates in the two tangential dimensions are half as large.

The value of T_{30} required to achieve this Δr , strain and strain rate depends on the strength S_b ; conversely, the strength inferred from an experimental measurement of Δr depends on T_{30} . As a numerical example, if $S_b = 7 \times 10^8 \text{ erg/cm}^3$ (700 bars), a typical value for pure copper, then for the preceding parameters $T_{30} = 1.06 \times 10^{10} \text{ erg/cm}^3$ (10.6 kbar). In practice, smaller values of T_{30} are required for smaller $\Delta r/r_0$ and $\delta r/\delta r_{piezo}$; these are experimentally feasible, but if $\delta r_{piezo} \ll r_0$ then the simple analytic result is inapplicable. It should also be remembered that S_b will be affected by work hardening if $\delta r/r_0$ is not very small; in practice, strength models incorporating work hardening and thermal effects and a quantitative treatment of the elastic and piezoelectric response would be required and numerically integrated.

3. Power Supply

The piezoelectric equations yield the relation between the radial electric field E_3 and the normal component of stress T_3 on a spherical surface:

$$E_3 = -\frac{T_3}{d_{33}c_{33} + 2d_{13}c_{13}}. \quad (\text{C16})$$

Substituting typical values of the elastic and piezoelectric coefficients for PZT yields the estimate (in MKS units, for convenience)

$$E_3 \approx -T_3 \times 0.08 \frac{\text{V}}{\text{m-Pa}}. \quad (\text{C17})$$

To achieve a nominal $T_3 = 10^7$ Pa (100 bars) requires $E_3 \approx 10^6$ V/m, a value comparable to coercive field of PZT piezoelectrics, and approximately the maximum field at which their piezoelectric response remains unsaturated. At high frequencies the coercive field may be higher, but is likely to be of the same order of magnitude. The potential drop across the previously assumed shell of piezoelectric 0.3 cm thick is then $V = 3$ kV.

The capacitance of the piezoelectric is

$$C = 4\pi\kappa\epsilon_0 \frac{r_0(r_0 + \delta r_{\text{piezo}})}{\delta r_{\text{piezo}}} \approx 0.5 \mu\text{F}, \quad (\text{C18})$$

where we have taken the relative dielectric constant (at zero strain) of PZT $\kappa_{33} = 1000$, a representative value. The energy required to charge it to the required potential

$$\mathcal{E} = \frac{CV^2}{2} \approx 2.2 \text{ J}. \quad (\text{C19})$$

Charging must be accomplished in a time $t_{\text{charge}} \ll 1/b$, and implies a current

$$J \simeq \frac{CV}{t_{\text{charge}}} \gg CVb \simeq 3 \times 10^3 \text{ Amp}, \quad (\text{C20})$$

or a charging power

$$P \simeq JV \gg \frac{CV^2b}{2} \simeq 5 \times 10^6 \text{ W}. \quad (\text{C21})$$

The implied impedance

$$Z \equiv \frac{V}{J} \ll \frac{1}{Cb} \simeq 1 \Omega. \quad (\text{C22})$$

These parameters are not challenging for a high voltage capacitive pulsed power supply.

4. Transient Piezoelectric Response

Piezoelectrics are described by their static displacement coefficients d_{33} describing the ratio of strain parallel to electric field applied in the poling direction (denoted by 3), $d_{31} = d_{32}$ (negative) the ratio of strain in the transverse (1 and 2) directions to the electric field applied in the poling direction, and d_{15} the ratio of shear in the 13 plane to electric field applied in the transverse direction. Symmetry implies values for other coefficients. This is a quasi-static description.

We are concerned with fields applied much faster than the elastic relaxation time of the piezoelectric. When such a field is applied, there is an immediate increase in stress, but strain follows only more slowly, on the time scale of the acoustic transit time across the piezoelectric, and in general the deformation is oscillatory as the initial stress distribution excites elastic waves. The immediate stress is the stress field that would return the quasi-statically strained configuration to its unstrained (zero electric field) state.

The quasi-static strain is

$$\mathbf{u} = \begin{vmatrix} d_{13}E_3 & 0 & 0 \\ 0 & d_{13}E_3 & 0 \\ 0 & 0 & d_{33}E_3 \end{vmatrix}, \quad (\text{C23})$$

where the electric field $\vec{E} = E_3\hat{z}$. Using the relation between stress and strain,

$$\sigma_{ik} = Ku_{ll}\delta_{ik} + 2\mu\left(u_{ik} - \frac{1}{3}\delta_{ik}u_{ll}\right), \quad (\text{C24})$$

where K is the bulk modulus and μ the shear modulus.

We first consider an unconstrained piezoelectric. Then the stress state that produces these strains is

$$\sigma_{22} = \sigma_{11} = K(2d_{13} + d_{33})E_3 + 2\mu\left(\frac{1}{3}d_{13} + \frac{1}{3}d_{33}\right)E_3 \quad (\text{C25})$$

$$\sigma_{33} = K(2d_{13} + d_{33})E_3 + 2\mu\left(\frac{2}{3}d_{33} - \frac{2}{3}d_{13}\right)E_3, \quad (\text{C26})$$

where E_3 is the magnitude of the electric field in the 3-direction.

If the constraint $u_{11} = u_{22} = 0$ is imposed, as appropriate for a spherical shell in which the 3-direction of poling and electrification is radial, an additional stress field σ' must be added:

$$\sigma'_{22} = \sigma'_{11} = d_{13}E_3 \left[2K(\nu - 1) + 2\mu\left(-\frac{1}{3} - \frac{2}{3}\nu\right)\right] \quad (\text{C27})$$

$$\sigma'_{33} = d_{13}E_3 \left[2K(\nu - 1) + 2\mu\left(\frac{2}{3} + \frac{4}{3}\nu\right)\right]. \quad (\text{C28})$$

Combining these, the radial component of stress that acts on the shell pushed by the piezoelectric

$$\sigma_{33} = KE_3(2\nu d_{13} + d_{33}) + 2\mu E_3 \left(\frac{4}{3}\nu d_{13} + \frac{2}{3}d_{33} \right). \quad (\text{C29})$$

5. Estimates

Using Eqs. C14 and C16 we estimate the electric field, assuming linear piezoelectric response, required to produce significant plastic flow. We take an inward plastic displacement of the test sample $\Delta r = 0.3r_0$ and a sample thickness $\delta r = 0.3\delta r_{piezo}$; for example, a sample with initial radius $r_0 = 1$ cm and initial thickness $\delta r = 1$ mm surrounded by a piezoelectric $r_{piezo} = 3$ mm thick. For representative parameters of PZT piezoelectric ceramic and a test sample of copper with $S_b = 7 \times 10^8$ erg/cm³ (700 bars) we require $E_3 = 3 \times 10^7$ V/m, while even for very soft indium with $S_b = 9 \times 10^6$ erg/cm³ (9 bars)²⁶ we require $E_3 = 3.6 \times 10^6$ V/m. Both these values far exceed the fields of about 5×10^5 V/m at which piezoelectrics saturate and depole. Piezoelectric drive cannot be strong enough to plastically deform even very soft metals.

REFERENCES

- ¹Hopkinson, G., *Phil. Trans. Roy. Soc. (London) A* **213**, 437–456 (1914).
- ²Kolsky, H., *Proc. Phys. Soc. London B* **62**, 676–701 (1949).
- ³Davies, R. M. *Phil. Trans. Roy. Soc. (London) A* **240**, 375–457 (1948).
- ⁴Taylor, G. *Proc. Roy. Soc. London A* **194**, 289–299 (1948).
- ⁵Gurson, A. L., *J. Eng. Matl. Tech.* **99**, 2–15 (1977).
- ⁶Follansbee, P. S., *Metallurgical Applications of Shock-Wave and High-Strain-Rate Phenomena* eds. L. E. Murr, K. P. Staudhammer and M. A. Meyers (Marcel Dekker, New York, 1986) 451–479.
- ⁷Huang, S., and Clifton, R. J., *Macro and Micro-Mechanics of High Velocity Deformation and Fracture, IUTAM Symp., Tokyo 1985* eds. K. Kawata and J. Shioiri (Springer-Verlag, Berlin, 1987) 63–73.
- ⁸Lesuer, D. R., LeBlanc, M. M., and Kay, G. J., *UCRL-53868-98* 6-7-6-15 (1998). *N.B.:* This report contains a number of typographical errors: The caption to Fig. 7 misidentifies

the material and the single high strain rate data point is placed at a position inconsistent with its stated strain rate.

- ⁹Horstemeyer, M. F., Baskes, M. I., and Plimpton, S. J., *Acta Materialia* **49**, 4363–4374 (2001).
- ¹⁰Williamson, G. K., and Smallman, R. E., *Phil. Mag. Ser. 8* **1**, 34–46 (1956).
- ¹¹Steinberg, D. J., Cochran, S. G., and Guinan, M. W., *J. Appl. Phys.* **51**, 1498–1504 (1980).
- ¹²Steinberg, D. J., and Lund, C. M., *J. Appl. Phys.* **65**, 1528–1533 (1989).
- ¹³Razorenov, S. V., Savinykh, A. S., Kanel, G. I., and Skakun, S. N., *Shock Compression of Condensed Matter—2003, AIP Conf. Proc.* **706**, 491–494 (2004).
- ¹⁴Wilkins, M. L., *Meth. Comp. Phys.* **3**, 211–263 (1964).
- ¹⁵Landau, L. D., and Lifshitz, E. M., *Theory of Elasticity*, 1st Ed. (Addington-Wesley, Reading, Mass., 1959), pp. 20–21.
- ¹⁶*Explosive Properties of Gaseous Mixtures Containing Hydrogen and Chlorine* The Chlorine Institute Pamphlet 121 <https://bookstore.chlorineinstitute.org/pamphlet-121-explosive-properties-of-gaseous-mixtures-containing-hydrogen-and-chlorine.html> (2016).
- ¹⁷Gibson, G. E., and Bayliss, N. S., *Phys. Rev.* **44**, 188 (1933).
- ¹⁸Gibson, G. E., Rice, O. K., and Bayliss, N. S., *Phys. Rev.* **44**, 193 (1933).
- ¹⁹<https://webbook.nist.gov/cgi/cbook.cgi?ID=C7647010\&Mask=1000\#Diatomic> accessed Aug. 15, 2018.
- ²⁰Moyle, M. P., Morrison, R. B., and Churchill, S. W., *A. I. Ch. E. Journal* **6**, 92 (March 1960).
- ²¹Benham, R. A. Preliminary Experiments Using Light-Initiated High Explosive for Driving Thin Flyer Plates SAND-79-1847 (1980).
- ²²Benham, R. A. Initiation and Gas Expansion Model for the Light-Initiated High Explosive Silver Acetylide–Silver Nitrate SAND-79-1829 (1980).
- ²³Sourcebook on the Light-Initiated High Explosives Facility, Sandia National Laboratory, Albuquerque, N. Mex. <http://fas.org/man/eprint/lhef.pdf> accessed Jan. 4, 2018.
- ²⁴Covert, T. Light-Initiated High Explosives (LIHE) Test Technique and Capabilities, 16th APS Topical Conference on Shock Compression of Condensed Matter E3.00003 Nashville, Tenn. 2009 <http://meetings.aps.org/link/BAPS.2009.SHOCK.E3.3>. accessed Jan. 4, 2018.

- ²⁵Reichmann, K., Völkl, E., Ahrens, M., Fleig, J., and Vötsch, J., *J. Matl. Sci.* **45**, 1473–1477 (2010).
- ²⁶Reed, R. P., McCowan, C. N., Walsh, R. P., Delgado, A. and McColskey, J. D., *Mat. Sci. Eng. A* **102**, 227–236 (1988).